Theory of ultrafast autoionization dynamics of Fano resonances

W.-C. Chu* and C. D. Lin

J. R. Macdonald Laboratory, Department of Physics, Kansas State University, Manhattan, Kansas 66506, USA

(Received 5 September 2010; published 29 November 2010)

We study atomic autoionization processes in the time domain. With the emerging attosecond extreme vacuum ultraviolet and soft x-ray pulses, we first address how to characterize the time evolution of the decay of a discrete state into a degenerate continuum. A short pump beam generates a number of resonance states in a series and the nearby background continuum, and the resultant wave packet evolves with time until the full decay of the bound states. Taking the $2pns(^1P^o)$ resonance series embedded in the $2s\epsilon p(^1P^o)$ continuum in a beryllium atom as an example, the time evolution of the autoionizing wave packet in the energy domain and in coordinate space is calculated and analyzed, where Fano profiles build up in the photoelectron energy during the process. A proposed pump-probe scheme assumes that the probe beam ionizes the $2s$ inner electron in the wave packet. The lifetimes of the resonances and the photoelectron energy distribution can be obtained from the ionization yield vs. the time delay of the probe.

DOI: 10.1103/PhysRevA.82.053415 PACS number(s): 32.80.Zb, 32.80.Fb

I. INTRODUCTION

Scattering processes—photoionization, electron collision, etc.—have been important tools for studying physical systems since the early days of the development of atomic theories. Autoionization, first observed by Beutler [1] in the photoabsorption of rare gas atoms, is a phenomenon where the energy spectrum is characterized by asymmetric resonance peaks, which were explained by Fano in his seminal paper in 1961 [2]. In this paper, asymmetric resonance in photoabsorption occurs in the energy region where a discrete state is embedded in the continuum. Photoabsorption populates both the discrete state and the continuum states. The interaction of the discrete state with the continuum results in the "autoionization" of the former, where the discrete state interferes with the directly populated continuum states to form asymmetric Beutler-Fano profile. Today, Fano resonances have been used to describe a wealth of physical phenomena in atomic, molecular, and optical systems, condensed matter systems [3,4], nanostructures [5], and many other fields. Essential to Fano's theory is that each resonance can be characterized by three parameters, the "unshifted" resonance position E_r, the shape parameter q, and the resonance width Γ. The resonance width characterizes the decay time or the lifetime of the discrete state. Since the typical resonance width of an atomic or molecular system is of the order of 10^{-1} eV, which corresponds to a lifetime as short as a few femtoseconds, almost all measurements on these resonances have been carried out in the energy domain, using high-resolution spectroscopy. Today a large set of experimental and theoretical data on these resonances has been collected, and they provide important structural information of the systems.

In the past decade, with the advent of laser technology, single attosecond pulses (SAPs) are becoming available [6]. Such pulses opened up a new research platform for studying electronic dynamics, such as autoionization dynamics. Indeed, the first SAP experiment in an atomic system was to determine the lifetime of the Auger decay of an M-shell hole in Kr created by an extreme vacuum ultraviolet (XUV) attosecond pulse by Drescher *et al.* [7]. For Auger decay, the resonance profile is mostly symmetric, and thus only the decay width or the lifetime of the inner-shell hole was determined. In Ref. [7], the lifetime is determined by creating the inner-shell hole in the presence of an IR laser. By changing the time delay between the XUV pulse and the IR, photoelectron spectra can be used to "deduce" the lifetime of the inner-shell hole—based on the approximate "streaking" theory [8]. This streaking theory has been generalized to Fano resonances by Zhao and Lin [9] as well as by others [10,11]. However, the photoelectron spectra from this XUV + IR setup are very complicated and only the lifetime of the Fano resonance can be extracted.

Due to the insufficient fluence of the SAPs so far, existing measurements using attosecond pulses for Auger decay or autoionization have all been carried out using the XUV + IR pump-probe setup where the two pulses actually overlap in time [7,12,13]. Rigorously speaking, the IR is not probing the resonances created by the attosecond XUV pulse in these experiments since the photoelectron is created in the IR field. With improved technology in attosecond pulse generation and the recent advances in x-ray free-electron lasers, we envision that intense attosecond pulses will become available in the near-future, such that a true time-dependent investigation of the autoionization process will be possible. In this article, we analyze the time evolution of a Fano resonance or the autoionization dynamics of the system in the field-free condition before the discrete state fully decays into the continuum. For example, if the discrete state has a lifetime of 20 fs while the pump pulse is only 1.5 fs, we ask what is the time evolution of the wave packet associated with the decay process after the pump pulse and how the energy profile eventually evolves into what is characterized by the Fano resonance shape.

We comment that the time evolution of a Fano resonance has been studied in several calculations by solving the time-dependent Schrödinger equation of helium or a model atom [10,14–16], with or without an IR probe. These studies did not address how to retrieve the time evolution of the resonance profiles. Similarly, autoionization of double Rydberg states on the time scale of picoseconds has been studied [17].

*wcchu@phys.ksu.edu

In the meanwhile, the interaction of a doubly excited state with a whole Rydberg series also falls into a similar category [18,19]. Understanding the time evolution of two-electron wave packets and the issue of how to probe their evolution lie at the heart of understanding and controlling two-electron dynamics.

In this article, we use two pulses that are separate in time. The probe is always placed strictly after the pump so that the field-free evolution between the pulses can be defined. The physical process is understood roughly as the decaying of the bound state to the continuum due to the interaction between them. In Sec. II, starting with Fano theory, which is for stationary states, we construct a time-dependent wave function of the system which describes the time evolution of the electron wave packet after the pump pulse. The wave function is recast in the basis set of the bound state and the continuum states, where it contains the time information for the bound and the continuum components. The wave packet for the continuum part is shown to evolve to the typical Fano resonance profile over a long time. We thus define the continuum wave packet over a short time as the time-dependent Fano profile of the autoionization. Since the pump pulse is short, it inevitably spans a broadband in the energy spectra. Assuming that the background energy spectrum generated by the pump is described by a Gaussian distribution, we generalize the theory to include all resonances within the bandwidth. In Sec. III we apply our theory to the resonances in beryllium to investigate wave packet dynamics after the pump pulse. In Sec. IV we demonstrate how to probe time-dependent Fano resonances, using the example of beryllium given in Sec. III. A short summary and future outlook are given in Sec. V.

II. THEORY

A. Fano's theory of resonance

In a multielectron atomic system, high-lying discrete states are embedded in the continuous spectrum if these discrete energies are higher than the binding energy. Both the bound and the continuum states are described in terms of configurations. According to Ref. [2], with one bound state and its nearby continuum, the system is governed by the total Hamiltonian given by

$$\langle\alpha|H|\alpha\rangle = E_r, \tag{1}$$

$$\langle\beta_E|H|\alpha\rangle = V_E, \tag{2}$$

$$\langle\beta_{E'}|H|\beta_E\rangle = E\delta(E'-E), \tag{3}$$

where $|\alpha\rangle$ and $|\beta_E\rangle$ are the bound and continuum configurations, respectively. The off-diagonal terms V_E represent the mixing strength between the bound and the continuum. The diagonal terms E_r and E are the bound and continuum energies, respectively.

The eigenstates $|\psi_E\rangle$ of the atom are obtained by diagonalizing the Hamiltonian in Eqs. (1)–(3) and are given by Fano as

$$|\psi_E\rangle = a_E|\alpha\rangle + \int b_{EE'}|\beta_{E'}\rangle dE', \tag{4}$$

where the coefficients are

$$a_E = \frac{\sin\Theta}{\pi V}, \tag{5}$$

$$b_{EE'} = \frac{1}{\pi}\frac{\sin\Theta}{E-E'} - \delta(E-E')\cos\Theta, \tag{6}$$

$$\Theta \equiv -\arctan\frac{\pi V^2}{E-E_r}. \tag{7}$$

Here we assume that $V_E = V$ is a real constant in the narrow energy region for each Fano resonance, provided that the bound and the continuum states are in real representation.

Originally Fano's theory was applied to photoabsorption processes. The transition amplitude is $c_E \equiv \langle\psi_E|T|g\rangle$, where $|g\rangle$ is the ground state, $|\psi_E\rangle$ is the excited state of energy E, and T is the photon transition operator. States $|g\rangle$ and $|\psi_E\rangle$ are eigenstates of the atomic Hamiltonian H, so the coefficients c_E do not change with time. In Ref. [2], the continuum wave functions are taken to be real standing waves. The absorption cross section is proportional to $|c_E|^2$, which contains the features of Fano profiles. Until recently, all photoabsorption measurements are performed using light sources of hundreds of picoseconds or longer, where they can be considered monochromatic. Thus, $|\psi_E\rangle$ of a single E is promoted in each measurement. To trace out a Fano resonance, monochromatic lights are tuned across the resonance while the cross section for each energy point is recorded.

Although Fano's theory was applied to photoabsorption originally, it can be trivially generalized to study photoelectron angular distributions. While the continuum functions in Eq. (4) are taken to be real standing waves, $|\psi_E\rangle$ is an eigenstate of the Hamiltonian. To obtain the scattering amplitude for an electron with momentum $\vec{k}$, one only needs to project the standing wave onto the momentum eigenstate $\vec{k}$ of the photoelectrons, given, in energy-normalized form, by

$$\psi_{\vec{k}}(\vec{r}) = \sqrt{\frac{2}{\pi k}}\frac{1}{r}\sum_{lm} i^l e^{i\eta_l} u_l(kr) Y_{lm}(\hat{r}) Y^*_{lm}(\hat{k}). \tag{8}$$

Here $u_l(kr)$ are the radial wave function of the electron taken as real standing waves as in Fano's theory, η_l are the total scattering phase shifts, and the Ys are spherical harmonic functions.

Following the notation in Ref. [2], the width of the resonance is defined by $\Gamma \equiv 2\pi V^2$. Assuming that $\langle\beta_E|T|g\rangle$ is energy independent near the resonance energy E_r, the q parameter is defined by

$$q \equiv \frac{\langle\alpha|T|g\rangle}{\pi V\langle\beta_E|T|g\rangle}. \tag{9}$$

Without the flat-background and the constant-V assumptions, $|\alpha\rangle$ will be replaced by the "modified bound state" defined in Ref. [2], which contains a term based on uneven V_E and $|\beta_E\rangle$ near E_r. We assume that this modification is negligible in general cases and consider the q parameter as defined in Eq. (9). Fano's theory predicts the resonance profile in a simple form, where the associated parameters E_r, Γ, and q can be extracted by fitting the form to the measured profile.

With the advent of available light pulses of a few femtoseconds or shorter, one can use such a short pulse to ionize the atom. After the pump pulse is over, the time-dependent wave

function of the atom is given by

$$|\Psi(t)\rangle = c_g e^{-iE_g t}|g\rangle + \int c_E e^{-iEt}|\psi_E\rangle dE, \qquad (10)$$

where, in a single pulse, the integral in Eq. (10) covers a bandwidth more than the width of a resonance. Such a resonance can be measured, long after the pump, in a high-resolution spectrometer. This amounts to projecting out the time-dependent wave function $|\Psi(t)\rangle$ over a long time. Thus the whole Fano resonance is generated in a single pulse and its profile is given by $|c_E|^2$.

We now consider the situation where the pump pulse is shorter than the lifetime of a Fano resonance. One would like to "see" the dynamics of the autoionization. However, this information is not contained in $|c_E|^2$ since $|\psi_E\rangle$ are eigenstates of the atomic Hamiltonian and the coefficients c_E are constant when the pump field is absent. Thus in Eq. (10), the time information is hidden and not recognized, even though we "know" that autoionization is happening!

B. Time-dependent wave function in a configuration basis

It is convenient to define the excited wave function $|\Psi_{\rm ex}(t)\rangle$ as the total wave function $|\Psi(t)\rangle$ excluding the ground-state part since the ground state does not participate in autoionization. Instead of using eigenstates as expressed in Eq. (10), we alternatively expand the excited wave function in a configuration basis as

$$|\Psi_{\rm ex}(t)\rangle = d_\alpha(t)|\alpha\rangle + \int d_E(t)|\beta_E\rangle dE. \qquad (11)$$

Since $|\alpha\rangle$ and $|\beta_E\rangle$ are not eigenstates of the atomic Hamiltonian, the coefficients $d_\alpha(t)$ and $d_E(t)$ are time dependent. One expects that at a long time (compared to the lifetime), the coefficient $d_\alpha(t)$ will go to 0 and all the information on the total wave function will be contained in $d_E(t)$. However, the time evolution of these coefficients cannot be measured in the laboratory: they change over a time scale of femtoseconds or less, while laboratory electronics can only measure changes of the order of picoseconds or longer. Here we define $|d_E(t)|^2$ as the "time-dependent Fano resonance profile" or, in short, the "resonance profile." Here we discuss how these coefficients behave. The measurement issues are addressed later.

Assuming that the initial values of $d_\alpha(t)$ and $d_E(t)$ are known, with the aid of Eqs. (4)–(7), the time-dependent coefficients are solved and given by

$$d_\alpha(t) = \left[d_\alpha^{(0)} e^{-\frac{\Gamma}{2}t} + \int d_E^{(0)} g_E(t) dE\right] e^{-iE_r t}, \qquad (12)$$

$$d_E(t) = \left[d_\alpha^{(0)} g_E(t) + \int d_{E'}^{(0)} f_{EE'}(t) dE'\right] e^{-iE_r t} + d_E^{(0)} e^{-iEt}, \qquad (13)$$

where the functions $g_E(t)$ and $f_{EE'}(t)$ are defined by

$$g_E(t) \equiv \frac{V}{E - E_r + i\Gamma/2}[e^{-i(E-E_r)t} - e^{-\frac{\Gamma}{2}t}], \qquad (14)$$

$$f_{EE'}(t) \equiv \frac{V}{E - E'}[g_E(t) - g_{E'}(t)]. \qquad (15)$$

The superscript (0) denotes the initial values, that is,

$$d_\alpha^{(0)} = \langle\alpha|\Psi(0)\rangle, \qquad (16)$$

$$d_E^{(0)} = \langle\beta_E|\Psi(0)\rangle. \qquad (17)$$

The solutions in Eqs. (12)–(15) are calculated exactly for a given set of parameters $d_\alpha^{(0)}$, $d_E^{(0)}$, E_r, and Γ, where these parameters can be either obtained by running a separate program such as the time-dependent Schrödinger equation code or time-dependent perturbation calculation, based on prior knowledge of the pump, or extracted from the experimental values in the time-integrated spectrum. In the latter case, with q defined by Eq. (9) and rewritten as

$$q \equiv \left.\frac{d_\alpha^{(0)}}{\pi V d_E^{(0)}}\right|_{E=E_r}, \qquad (18)$$

the initial coefficient $d_\alpha^{(0)}$ can be extracted since the value of q and the background magnitude of $d_E^{(0)}$ can be obtained from the Fano profile after a long time [the phase of $d_E^{(0)}$ can be deduced if photoelectron angular distributions are measured]. Equations (12)–(15) are the backbone of our model.

Note that the initial coefficients $d_\alpha^{(0)}$ and $d_E^{(0)}$ are, in general, complex values, while q is real. Within the narrow range of a resonance width, the energy E in $d_E^{(0)}$ is close to the bound-state energy E_r such that the phases of $d_\alpha^{(0)}$ and $d_E^{(0)}$ are assumed to be the same in the neighborhood of the resonance, and the corresponding q, representing the ratio between $d_\alpha^{(0)}$ and $d_E^{(0)}$, is real. When $d_E^{(0)}$ spans a wide energy range covering many resonances, its phase varies smoothly with E, but in each resonance region, the preceding statement is still true, and each q is real.

The decay lifetime of the bound state is defined as $T \equiv 1/\Gamma$. Rigorously speaking, the dynamics of the autoionization is about not only the decay of the bound state, but also its coupling to the continuum [see Eq. (11)]. The wave packet can propagate from the continuum to the bound state or the other way around, or between continuum states of different energies through the bound state. Thus, the lifetime T, determined by the interaction matrix V, characterizes the time scale of the whole event.

We can generalize Eqs. (12)–(15) to include multiple resonances by applying Fano's theory for many bound states [2] and assuming that higher-order perturbation by V is negligible. The excited wave function is

$$\Psi_{\rm ex}(t) = \sum_n d_n(t)|\alpha_n\rangle + \int d_E(t)|\beta_E\rangle dE, \qquad (19)$$

with the coefficients given by

$$d_n(t) = \left[d_n^{(0)} e^{-\frac{\Gamma_n}{2}t} + \int d_E^{(0)} g_{nE}(t) dE\right] e^{-iE_n t}, \qquad (20)$$

$$d_E(t) = \sum_n \left\{\left[d_n(t) g_{nE}(t) + \int d_{E'}^{(0)} f_{nEE'}(t) dE'\right] e^{-iE_n t}\right\} + d_E^{(0)} e^{-iEt}, \qquad (21)$$

where the label n is the index for the nth bound state. The g function and the f function, now subscripted with n,

are calculated independently for each resonance, with the associated parameters as given by Eqs. (14) and (15).

To simulate the effect of the finite range of V while keeping the calculation simple, the profiles can be further adjusted by multiplying each "resonance term" in Eq. (21) (in the curly braces) by a Gaussian window function to limit the range of each resonance. For an isolated resonance, the effect of the window function is minimum or unnecessary because the window function mainly removes "the wings," but not the center, of the resonance, where the central part is the significant and informative part. In contrast, when dealing with many resonances, without the window functions, the wings may be overly extended and unnaturally perturb the nearby resonances. In the latter case, multiplying the window functions is an effective and efficient solution.

1. Flat initial continuum (IC) distributions

To study the qualitative behavior of the wave function, we first assume that the initial profile is flat, that is, $d_E^{(0)} = \text{const}$. This initial continuum, dubbed IC_1, is valid near the resonance positions if the pump bandwidth is broad enough relative to the resonance widths that the populated profile is nearly flat around E_r. For conceptual presentation, only the single-resonance formulas, Eqs. (12)–(15) are referred to here, while the idea is the same for the many-resonance case. Defining the scaled time s as $s \equiv \Gamma t$ and the scaled energy ϵ as $\epsilon \equiv 2(E - E_r)/\Gamma$, the bound and the continuum coefficients under the IC_1 are

$$d_\alpha(s) = d_\alpha^{(0)} \left(1 - \frac{i}{q}\right) e^{-\frac{1}{2}s}, \tag{22}$$

$$d_\epsilon(s) = d_\epsilon^{(0)} \frac{1}{\epsilon + i}[(q + \epsilon)e^{-\frac{i}{2}\epsilon s} - (q - i)e^{-\frac{1}{2}s}], \tag{23}$$

where, in the scaled energy, the q parameter becomes

$$q \equiv \frac{d_\alpha^{(0)}}{\pi V d_\epsilon^{(0)}}, \tag{24}$$

and the factor $e^{-iE_r t}$ disappears because ϵ is measured relative to the resonance energy. While the coefficients given by Eqs. (22) and (23) represent the evolution for $s > 0$, their limits at $s \to 0$ are different from the initial coefficients $d_\alpha^{(0)}$ and $d_\epsilon^{(0)}$ that we have defined at $s = 0$. This discontinuity means an immediate jump of the wave function right after evolution starts. This unphysical behavior is due to the integral of the g function in Eq. (14) and f function in Eq. (15) over infinite energy range at very short times, where contributions from E that are much higher or lower than E_r are misleadingly counted in, while in practice, only the energy range comparable to Γ should be considered. Nevertheless, the long-time behavior is reliable since both the g and the f functions are compressed more and more into the near-resonance region with increasing time.

In the $s \to \infty$ limit in Eqs. (22) and (23), the bound state decays to 0, but the continuum recovers the general form of the Fano profile:

$$\lim_{s\to\infty} |d_\epsilon(s)|^2 = |d_\epsilon^{(0)}|^2 \frac{|\epsilon + q|^2}{\epsilon^2 + 1}. \tag{25}$$

We emphasize that Eq. (25) is a mathematical consequence. It cannot be obtained from the measurement since continuum configurations are not eigenstates of the total atomic Hamiltonian. In the special case where $d_\alpha^{(0)} = 1$ and $d_\epsilon^{(0)} = 0$, the system starts with only the bound state, and the Lorentz profile will be recovered as $s \to \infty$; that is,

$$\lim_{s\to\infty} |d_\epsilon(s)|^2 = \frac{1}{\pi} \frac{1}{\epsilon^2 + 1}. \tag{26}$$

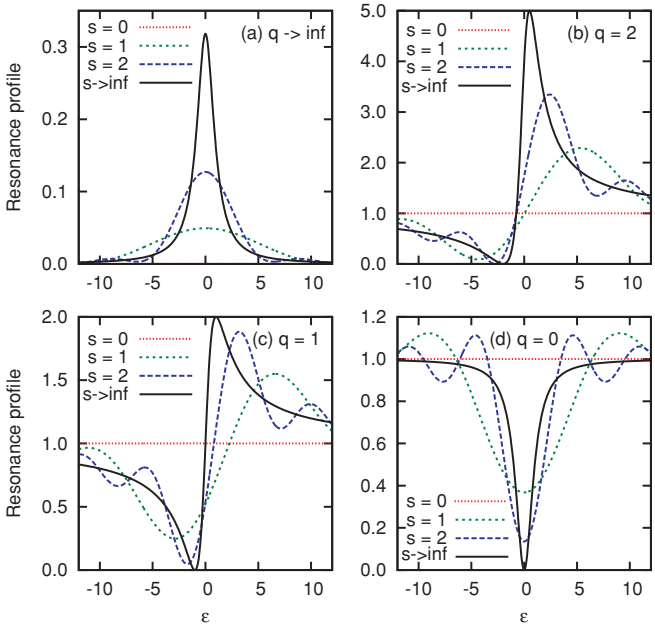

FIG. 1. (Color online) Resonance profile $|d_\epsilon(s)|^2$ calculated by Eq. (23) for (a) $q \to \infty$, (b) $q = 2$, (c) $q = 1$, and (d) $q = 0$. In (b)–(d), $|d_\epsilon^{(0)}|^2$ is normalized to 1. In all cases, the profile builds up with time, with small oscillations in energy, before reaching the final Fano profile.

Figure 1 shows the spectra at different times for $q \to \infty$, $q = 2$, $q = 1$, and $q = 0$. Each plot demonstrates how its spectrum morphs into the Fano profile. A feature found in the profile is the oscillation in the wings during evolution, which shrinks its energy period when the time increases, and disappears as $s \to \infty$. This oscillation, due to the phase between the two exponential terms in Eq. (23), is not seen in the conventional time-integrated spectra. Although analytically simple, the IC_1 simplification is conceptually rich and offers an easy visualization of the autoionization process.

2. Gaussian initial continuum distributions

The condition IC_1 is valid only in the vicinity of a resonance and is not applicable to the whole energy range. When a short pump pulse is used to initiate the system, one should cover its whole bandwidth and the state vectors must be properly normalized. Here we consider the normalization where the total probability for the bound component $\sum_n |d_n(t)|^2$ plus the continuum component $\int |d_E(t)|^2 dE$ is set to 1.0, where the ground state $|g\rangle$ is not considered since it is not involved in the autoionization. This normalization is automatically fulfilled by the exact solution once the initial coefficients are normalized. Additionally, we assume that the pump pulse has a Gaussian

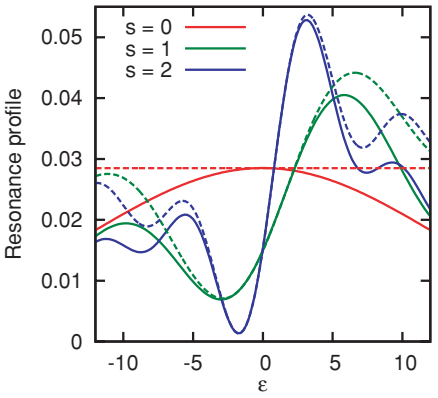

FIG. 2. (Color online) The resonance profile for the two ICs. Solid curves are carried out with the IC_2 defined by $q = 1$ and the FWHM bandwidth of 15Γ, or $D = 9\Gamma$. Dashed curves were carried out under the IC_1.

envelope, resulting in a Gaussian profile in energy. The initial coefficients are given by

$$d_n^{(0)} = \gamma q_n \pi V_n \exp\left[-\frac{1}{2}\left(\frac{E_n - \omega}{D}\right)^2\right], \tag{27}$$

$$d_E^{(0)} = \gamma \exp\left[-\frac{1}{2}\left(\frac{E - \omega}{D}\right)^2\right], \tag{28}$$

where

$$\frac{1}{\gamma^2} \equiv \sqrt{\pi} D + \sum_n (q_n \pi V_n)^2 \exp\left[-\left(\frac{E_n - \omega}{D}\right)^2\right]. \tag{29}$$

This initial continuum is dubbed the IC_2. The initial continuum state has a Gaussian energy distribution centered at ω with standard deviation D (FWHM $= 1.665D$). The initial coefficients are determined by the pump width and the resonance parameters E_n, Γ_n (or, equivalently, V_n), and q_n. For $D \gg \Gamma_n$, the IC_2 is reduced back to the IC_1 near the nth resonance. A comparison of the profiles under the IC_1 versus the IC_2 is plotted in Fig. 2 for $q = 1$, where the bandwidth (FWHM) for the IC_2 is 15Γ. As shown in Fig. 2, with the modification from the IC_1 to the IC_2, the $s = 0$ profile changes from a flat background to a Gaussian shape, and the $s = 1$ and $s = 2$ profiles change similarly. However, the featuring structures are preserved. The modification should be slight if the bandwidth is much wider than Γ, which is true for a sufficiently short pump.

3. *Growth and decay of a bound state*

Considering an isolated resonance, in the IC_1, the total bound state is an exponential decay function of time as described by Eq. (22). However, under the normalization condition of the IC_2, which is more realistic, the bound-state decay is not necessarily monotonic. For the IC_2 solution, the bound-state coefficient in Eq. (12) and its two terms are shown in Fig. 3 in their absolute squares. Figures 3(a) and 3(b) are for two initial bandwidths of the continuum centered at the resonance. The first term, which comes from the initial bound state, is always an exponential decay. The second term, which comes from the IC, goes through a rising period up to

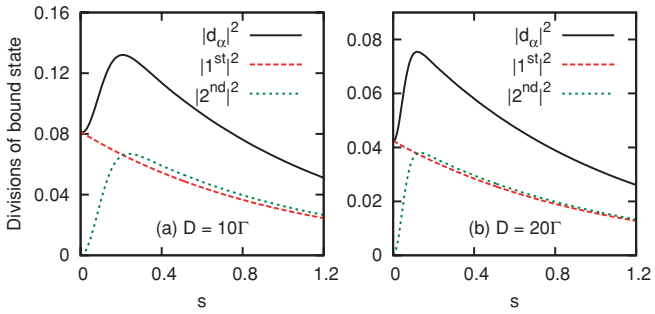

FIG. 3. (Color online) Bound-state coefficient defined by Eq. (12) and its compositions for $q = 1$ and (a) $D = 10\Gamma$ and (b) $D = 20\Gamma$, where D is the standard deviation of the pump beam (see Sec. II B 3). When D increases relative to Γ, the rising portion of the second term at the beginning of time gets shorter, and in the limit $D \gg \Gamma$, Eq. (22) (IC_1) is recovered.

about $s = 0.2$ in Fig. 3(a) and $s = 0.1$ in Fig. 3(b) before it decays. This rising period will shorten if the initial bandwidth increases or the pump duration shortens. In the limit of an infinite bandwidth, both the first and the second terms will be monotonic decay functions, and the solution in the IC_1 will be recovered. Note that even in a situation where the length of the rising period is comparable to the lifetime, such as Fig. 3(a) shows, the total bound-state population will eventually be dominated by the exponential decay. This growth part of the bound state is usually much shorter than the decay lifetime, so to "watch" this detail structure, a higher temporal resolution is required.

In the special case for $d_\alpha^{(0)} = 0$, the pump pulse does not directly populate the bound state of the system. The q parameter defined by Eq. (18) is 0. However, this definition is based on the assumption that V and the continuum background are constant near the resonance, and it excludes the modification term for the bound state. In an actual situation where no original bound state $|\alpha\rangle$ was populated, the theory needs to be modified to include higher-order terms. Nonetheless, even if we neglect the initial population of the original and the modified bound state, the time-dependent probability as given by Eq. (12) will still have a contribution from the initial continuum population $d_E^{(0)}$. In other words, we will still have the "decay" of the bound state even if it was not populated by the pump pulse. This somewhat awkward result is best understood in the following way. First, recall that the initial bound-state population depends on the transition operator connecting it to the ground state, while the "configuration interaction" V, which connects the bound state to the continuum, is always present. This "configuration interaction" feeds the bound state from the continuum, but the continuum states also draw the bound-state component and take it to large distances. If these continuum states were substituted with highly excited bound states, the outer electron would return to recollide with the inner electron(s) and repopulate the bound state. This would correspond to situations studied in Ref. [17–19]. To initiate the oscillation, the bound state does not have to be excited by the pump pulse. The ever-present "configuration interaction" is the one which is responsible for the oscillation. This "interaction" is the property of the Hilbert space but not of the specific excitation mechanism.

III. APPLICATION TO RESONANCES IN Be

In atomic systems, autoionization is understood only in the multiple-electron picture where electron-electron correlation is considered. Our theory is applied here to calculate the autoionizing wave packet of the $2p4s(^1P^o)$ resonance and of the $2pns(^1P^o)$ ($n = 3$ to 9) resonance series embedded in the $2sEp(^1P^o)$ continuum in the beryllium atom, generated by the photoionization from the $2s^2(^1S^e)$ ground state. For a short pump, we assume that the IC distribution can be approximated by a Gaussian distribution. Only the two outer electrons in beryllium are assumed to be active, and the $1s^2$ core electrons are frozen. The bound orbitals are Slater-type orbitals, where their analytical forms are determined by fitting the numerical Hartree-Fock calculations. The continuum basis functions are calculated with the model potential given in the literature [20] for $l = 1$ standing waves [21]. The resonance parameters are taken from the experiment by Wehlitz *et al.* [22], where E_r is 2.789 eV above the ionization threshold, $q = -0.52$, and $\Gamma = 0.174$ eV, or $T = 3.78$ fs. The pump beam has the carrier frequency right at the resonance and the duration of 2 fs, or a mean bandwidth of 0.912 eV.

For the $2p4s$ resonance case, the excited wave function, Eq. (11), is given by

$$\Psi_{\rm ex}(\vec{r}_1,\vec{r}_2;t) = d_{2p4s}(t)\phi_{2p4s}(\vec{r}_1,\vec{r}_2) + \int d_{E'}(t)\phi_{2sE'p}(\vec{r}_1,\vec{r}_2)\,dE', \qquad (30)$$

where the ϕ functions are constructed by corresponding bound orbitals and continuum waves, and symmetrized between the two electrons. The one-electron density is defined by

$$\rho(r_1,t) = \int\int |\Psi_{\rm ex}(\vec{r}_1,\vec{r}_2;t)|^2 r_1^2 r_2^2 d\Omega_1 d\Omega_2 dr_2, \qquad (31)$$

where the integral sums over the angular dependence as well as the radial part of one of the electrons. In the large-r region, $\rho(r_1,t)$ represents the electron density of the autoionizing electron. In this section, energy, time, and distance are in electronvolts (eV), femtoseconds (fs), and Bohr radius (a.u.), respectively, unless specified otherwise. The bandwidth in energy and the duration in time are defined in the FWHM.

First, we show how the wave packet moves in the coordinate space. Figure 4(a) displays the electron density at $t = 0$, 2, and 4 fs, where the time scale is about the lifetime of the resonance $T = 3.78$ fs. Before the propagation starts ($t = 0$), a dominant spatial distribution covers 0–60 a.u. This distribution is mainly contributed by the continuum, where the percentage initial bound state is as low as 7%. The spatial oscillation with a period of about 10–15 a.u., or a wave number of about 0.4–0.6 a.u., matches the energy distribution centered at the resonance energy of 2.789 eV. As time goes on, the electron wave packet moves outward toward large r. When the time is long compared with the autoionization lifetime, the motion of the electron wave packet can be analyzed more easily. In Fig. 4(b), the long-time behavior of the wave packet is plotted for $t = 40$, 80, 120, and 160 fs. The electron is always confined in some spatial range, but it gradually spreads wider when the time increases. By recognizing and tracing the two dominant peaks in Fig. 4(b) over time, we find that the corresponding velocities are almost constant. It is similar to a free electron

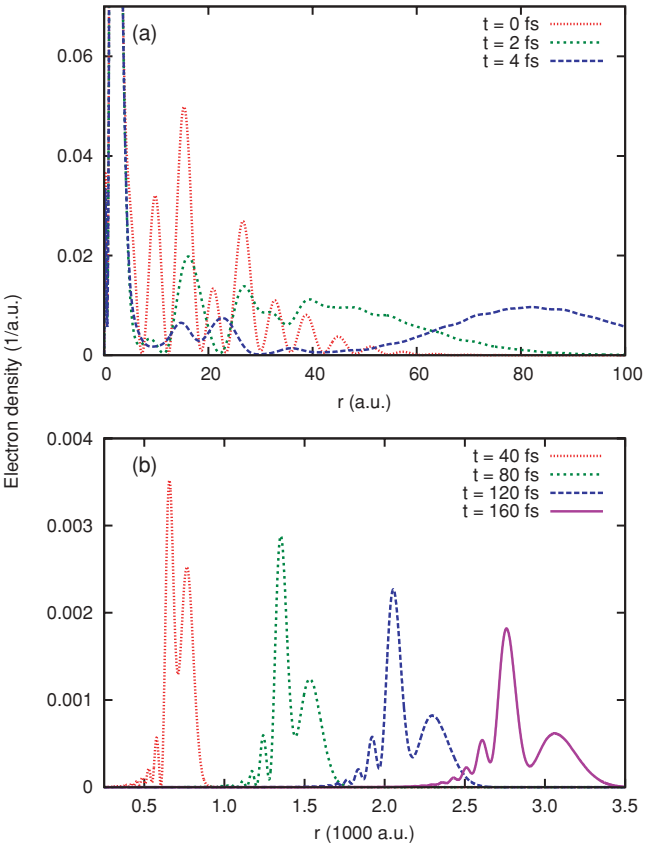

FIG. 4. (Color online) Electron density for the $2p4s$ resonance in Be with a pump pulse of 2 fs and central frequency at the resonance. The decay lifetime of the resonance is 3.78 fs. The electron density is shown for (a) short-time behavior, at $t = 0$, 2, and 4 fs, and for (b) long-time behavior, at $t = 40$, 80, 120, and 160 fs.

wave packet traveling in space, where its average velocity keeps the same, but its spatial distribution spreads. In this long time regime, the electron moves in a very predictable way to the large distance toward the detector.

Next, we discuss the evolution of the resonance profile $|d_E(t)|^2$, that is, the time-dependent Fano profile, for the same wave packet as in Eq. (30). In Fig. 5(a), the photoelectron energy profile is shown at $t = 0$, 1.5, 3, and 4.5 fs, that is, near the lifetime of the resonance $T = 3.78$ fs. The profile starts evolving with a Gaussian shape at $t = 0$ determined by the pump pulse and changes quickly within its lifetime. At $t = 4.5$, just a little longer than the lifetime, the double-peaked shape characteristic of autoionization can be seen, but the shape is not quite "settled" into the Fano profile. The long-time behavior is shown in Fig. 5(b). At $t = 10$ to 20 fs, the resonance profile is already quite close to the final Fano profile that can be determined in the standard energy domain measurements. It is also physically sensible that the electron velocities shown in Fig. 4(b) can be mapped onto, although not exactly, the energies of the two highest peaks in Fig. 5(b).

We have discussed an isolated resonance. Practically, a short pump pulse is likely to populate more resonances at once. Here we consider the case including the $2pns$ resonances up to $2p9s$ in Be. Even though the $2p2s$ state (about 5.277 eV above the ground state [23]) is lower than the $2s$ threshold and

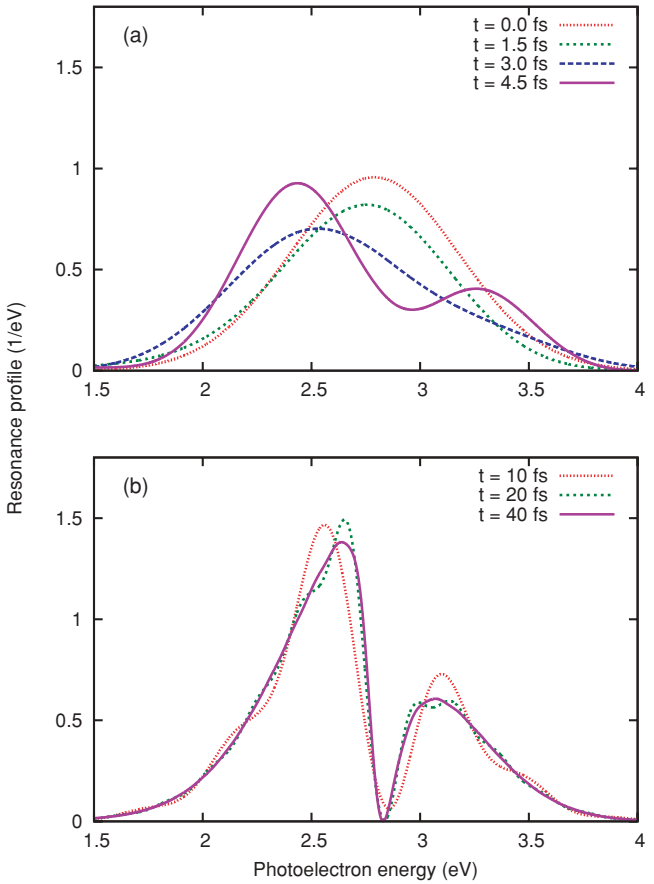

FIG. 5. (Color online) Resonance profile $|d_{E'}(t)|^2$ for the $2p4s$ autoionization in Be, at (a) $t = 0$, 1.5, 3, and 4.5 fs and at (b) $t = 10$, 20, and 40 fs.

will not show up in the continuum profile, it can, in general, interact with the continuum beyond the $2s$ threshold and is included in the present calculation. The parameters for these resonances are generated by setting $\mu = 0.6$, $\Gamma\nu^3 = 0.71$ eV, and $q = -0.8$, where μ is the quantum defect and ν is the effective quantum number. The first few widths, starting from $2p3s$, are 0.514, 0.181, 0.0833, and 0.0451 eV, and the decay lifetimes are 1.28, 3.64, 7.90, and 14.6 fs, respectively. The $2pns$ resonance series stretches between the $2s$ threshold and the $2p$ threshold, a range of about 4 eV. Our attention is directed at the time scale and energy scale of this series. The IC distribution is set to be centered at 2.3 eV above the ionization threshold, with a bandwidth of 1.825 eV, or pump duration of 1 fs. The bandwidth covering the resonances of interest is limited to the energy range above the $2s$ threshold to avoid unnecessary complications. Each resonance term in Eq. (21) is multiplied by a Gaussian window whose width is 2Γ to narrow down the interaction V to some finite range in the calculation. The resultant resonance profiles are displayed in Fig. 6, along with the experimental photoabsorption cross-section values in Ref. [22], plotted by the light-gray curve and normalized to fit in the vertical range of our calculation. The $2pns$ resonance series is shown in the experiment from low to high energy, starting with $2p3s$ at about 1.5 eV. For the calculation, Fig. 6 shows how the profiles evolve in time and are finalized, where the lower (wider) resonances build up

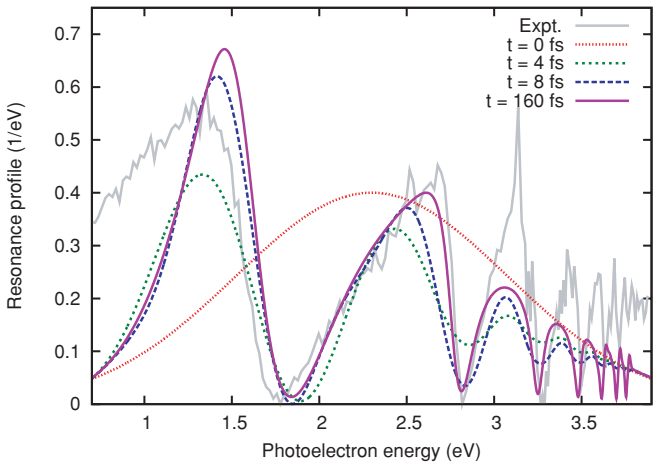

FIG. 6. (Color online) Calculated resonance profiles for the $2pns(^1P^o)$ resonances at $t = 0$, 4, 8, and 160 fs in Be, and experimental photoabsorption cross section in Be between the $2s$ and the $2p$ thresholds [22]. Experimental values are normalized to the vertical range of the calculation.

quickly and the higher (narrower) resonances slowly. At short times, the continuum must be viewed as a whole distribution which gives no information on individual resonances; only at long times, for example, $t = 160$ fs, the profiles assigned to individual resonances are shown. Nonetheless, our calculation and the experiment in Ref. [22] should not be compared with each other directly. In the present work, a short pump pulse covers a wide energy range; the system propagates coherently with time. In contrast, the experiment in Ref. [22] was done with many independent incoherent measurements, where each measurement was made for a single energy point using a long pulse of at least of hundreds of picoseconds and gives back a single quantity for the cross section.

We caution the readers that the time-dependent resonance profile shown in Fig. 6 is from theoretical calculations only, that is, a plot of $|d_E(t)|^2$ vs E for different time delays after the pump pulse. As emphasized earlier, $|d_E(t)|^2$ cannot be measured directly in the laboratory since any physical measurement will take at least many picoseconds, which cannot distinguish time evolution that happens on the femtosecond scale. In addition, the wave functions associated with the coefficients $d_E(t)$ in Eq. (19) are not eigenstates of the atom such that $|d_E(t)|^2$ cannot be directly interpreted as measurable probabilities.

IV. METHOD OF PROBING THE TIME-DEPENDENT AUTOIONIZATION PROCESSES

After we have predicted how the wave packet in the autoionization process evolves with time, an experimental scheme where such predictions can be confirmed is essential. Using a SAP pump and an IR probe, the lifetime of the Auger decay of an inner-shell hole [7] or of a Fano resonance in helium [12] have been "deduced." The streaking of an autoionizing electron in the IR laser field has been calculated by Wickenhauser *et al.* [10]. The streaked electron spectra are too complicated to allow the retrieval of the predicted intermediate profiles. Taking beryllium as an example, here

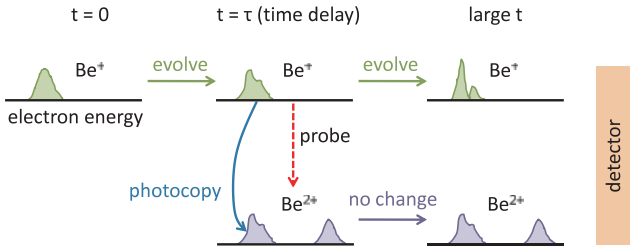

FIG. 7. (Color online) A conceptual scheme for probing the time-dependent resonance profiles. At $t = 0$ the pump pulse is over and autoionization starts while the system evolves freely. To determine the evolving electron wave packet at time τ, a probe pulse is used to ionize the $2s$ electron in the $2sEp$ continuum and create the $E'pEp$ states. After the probe is over, the new wave packet consists of a part of the old wave packet which continues to evolve and autoionize (upper row) and the newly generated part made of $E'pEp$ states (lower row). The latter does not change with time. By picking the responsible energy range and collecting the double-ionized signals, the resonance profile in the autoionization at moment τ is captured.

we propose a way to measure the time dependence of Fano profiles.

The probe scheme is sketched in Fig. 7. After the pump, we define the starting time for the autoionization as $t = 0$ such that the pump field is finished for $t > 0$. A probe pulse is shined onto the system with its peak at time delay τ. The probe has the duration of 1.5 fs, or bandwidth of 1.216 eV, and carrier energy ω of 40 eV. This probe pulse ionizes the $2s$ electron in the $2sEp$ continuum (binding energy of $2s$ is 18.21 eV). After the probe pulse is over, the excited wave packet in Eq. (30) changes to

$$|\Psi_{\rm ex}(t)\rangle = \sum_n d_n(t)|2pns\rangle + \int \bar{d}_E(t)|2sEp\rangle dE + \int\int d_{E'E}(t)|E'pEp\rangle dE'dE. \quad (32)$$

We have assumed that the $2pns$ bound states are not changed by the probe pulse, and only a small portion of the $2sEp$ continuum states is ionized [thus the amplitude now given by $\bar{d}_E(t)$ is slightly different from $d_E(t)$] to generate new $E'pEp$ states. After the probe pulse, both $d_n(t)$ and $\bar{d}_E(t)$ continue to change with time as the bound states decay. The newly created $E'pEp$ states are eigenstates of the atomic (field-free) Hamiltonian and are stationary states, and they can thus be probed by a laboratory detector. Using 40-eV probe pulses, the energy E' will be centered around 21.8 eV, well separated from the electron energy of 2.5 eV due to autoionization. Clearly the probability $|d_{E'E}(t)|^2$ should be independent of time and is proportional to $|d_E(\tau)|^2$. To determine $|d_E(\tau)|^2$ one can measure the energies of the two electrons in coincidence or by measuring the low-energy electrons in coincidence with Be^{2+} ions. Either way, the lower-energy group duplicates the original continuum profile at the moment of the probe. By changing the delay time of the probe, a copy of $|d_E(\tau)|^2$ can be determined. Due to the finite duration of the probe pulse, the measured copy of $|d_E(\tau)|^2$ will be somewhat smoothed out.

If the probe is of perturbative strength, we can calculate the predicted two-electron spectra quantitatively. In the presence

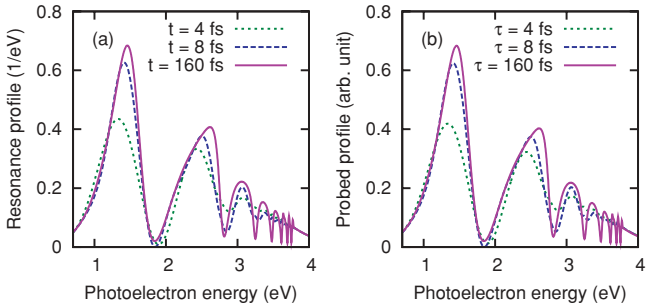

FIG. 8. (Color online) Time-dependent continuum profile compared with the probed profile in the Be case. (a) Calculation as specified in Fig. 6. (b) Retrieved profile using a probe beam with $\omega = 40$ eV and a duration (FWHM) of 1.5 fs. Signal values have been scaled to match the original profile at $t = 160$ fs. The agreement between (a) and (b) is good.

of the external probe field $\vec{F}_2(t)$, the coefficient for $E'pEp$ is given by the first-order time-dependent perturbation theory by

$$d_{E'E} = \langle E'pEp|U\left(\frac{T_0}{2}, -\frac{T_0}{2}\right)\left|\Psi_{\rm ex}\left(-\frac{T_0}{2}\right)\right\rangle \quad (33)$$

$$= \frac{1}{i}\int_{-\frac{T_0}{2}}^{\frac{T_0}{2}} \langle E'pEp|e^{-iH_0(\frac{T_0}{2}-t)}V_2(t)|\Psi_{\rm ex}(t)\rangle dt \quad (34)$$

$$= \frac{\mu}{i}\int_{-\frac{T_0}{2}}^{\frac{T_0}{2}} e^{-i(E'+E)(\frac{T_0}{2}-t)}F_2(t)\,d_{E'}(\tau+t)\,dt, \quad (35)$$

where $V_2(t)$ is the dipole interaction potential for the probe pulse. The interaction is turned on only for $-T_0/2 < t < T_0/2$. Note that t is now measured with respect to the center of the probe, and the total excited wave function $|\Psi_{\rm ex}(-T_0/2)\rangle$ at $t = -T_0/2$ has already gone through the autoionization process for a duration of $\tau - T_0/2$. In Eqs. (33) and (34), the time propagator $\exp[-iH_0(T_0/2+t)]$ in U operates on $\Psi_{\rm ex}(-T_0/2)$ and gives $\Psi_{\rm ex}(t)$ in return. In the next step in Eq. (35), since the bound states $2pns$ do not participate in the probe process, only the continuum part is written down. The dipole matrix element $\mu \equiv \langle E'p|z|2s\rangle$ is assumed to be a constant. The polarization of the probe field is in the z direction, that is, $\vec{F}_2(t) = \hat{z}F_2(t)$. The retrieved profile as a function of E is defined as $\int |d_{E'E}|^2 dE'$. Figure 8 shows very good agreement between the retrieved profile at different τ values and the original continuum profile at the associated time τ.

While the calculation given is in first-order perturbation, the scheme can be applied to an intense probe as well, as long as the probe field dominantly removes the $2s$ electron and has little effect on other components in the system. The Ep electron is not affected by the probe, and the continuum profile of $2sEp$ at τ will still be transferred to $E'pEp$ plainly (with additional peaks possibly from two-photon ionization). The advantage of a stronger probe is that it increases the signal rate. This may be an important factor to realize this pump-probe scheme since the population of double excited states by the pump can be already weak. In the present example, the photon energy is 11.62 eV for the pump and 40 eV for the probe, presuming that short UV sources are provided for both the pump and the probe.

V. CONCLUSIONS

In this paper we study the temporal behavior of the atomic autoionization process. Following the original paper of Fano, we treat autoionization as the decay of a discrete state into a degenerate continuum. Fano's theory characterizes such a resonance with a shape parameter q and a width Γ, in addition to the resonance energy position. For many decades, Fano resonances are measured and characterized in energy domain experiments. With the advent of XUV and soft x rays with pulse durations of attoseconds to a few femtoseconds, we address the question whether Fano resonances can be probed directly in the time domain within its typical lifetime. In particular, can we talk about the time-dependent Fano profiles before the discrete state is fully decayed, and can such profiles be measured experimentally?

To describe time-dependent Fano profiles, it is inconvenient to express the total time-dependent wave function in terms of the eigenstates of the system. Instead, the configuration basis states, including the bound and the continuum, used in Fano's original theory are much more useful (or more physical) for analyzing the autoionization process, and we are led to define the time-dependent Fano profiles by referring to the wave packets expanded in the continuum configuration basis states. To probe the temporal Fano profiles with a good time resolution, we suggest that the decay process be perturbed by a short soft-x-ray pulse which interrupts the autoionization at the time of the probe. The probe in the meantime creates a stationary wave packet that can be measured in the laboratory. We further consider many Fano resonances together if they fall within the bandwidth of the pump pulse.

The pump-probe scheme proposed here, requiring high-energy short pulses for both the pump and the probe, is not yet available today. However, attosecond technology is undergoing rapid growth, and the proposed scheme for measuring autoionization dynamics may become doable within a few years. At the same time, theory for attosecond electron dynamics is still a barren field today. General approaches to understanding electron dynamics for many-electron systems are badly needed at this time. Not all probe pulses are similarly effective in retrieving time-dependent wave packets. Without the general theoretical framework, it would be difficult to retrieve electron dynamics from the signals measured by the probe pulse.

ACKNOWLEDGMENT

This work was supported in part by Chemical Sciences, Geosciences and Biosciences Division, Office of Basic Energy Sciences, Office of Science, US Department of Energy.

[1] H. Beutler, Z. Phys. **93**, 177 (1935).
[2] U. Fano, Phys. Rev. **124**, 1866 (1961).
[3] J. Faist *et al.*, Nature (London) **390**, 589 (1997).
[4] V. Madhaven *et al.*, Science **280**, 567 (1998).
[5] A. E. Miroshnichenko, S. Flach, and Y. S. Kivshar, Rev. Mod. Phys. **82**, 2257 (2010).
[6] F. Krausz and M. Yu. Ivanov, Rev. Mod. Phys. **81**, 163 (2009).
[7] M. Drescher *et al.*, Nature (London) **419**, 803 (2002).
[8] M. Kitzler, N. Milosevic, A. Scrinzi, F. Krausz, and T. Brabec, Phys. Rev. Lett. **88**, 173904 (2002).
[9] Z. X. Zhao and C. D. Lin, Phys. Rev. A **71**, 060702 (2005).
[10] M. Wickenhauser, J. Burgdörfer, F. Krausz, and M. Drescher, Phys. Rev. Lett. **94**, 023002 (2005).
[11] O. Smirnova, V. S. Yakovlev, and A. Scrinzi, Phys. Rev. Lett. **91**, 253001 (2003).
[12] S. Gilbertson *et al.*, *International Quantum Electronics Conference (IQEC), Baltimore, Maryland, May 31, 2009* (Optical Society of America, Washington, DC, 2009).
[13] H. Wang, M. Chini, S. Chen, C. H. Zhang, Y. Cheng, F. He, Y. Cheng, Y. Wu, U. Thumm, and Z. Chang, Phys. Rev. Lett. **105**, 143002 (2010).
[14] Th. Mercouris, Y. Komninos, and C. A. Nicolaides, Phys. Rev. A **75**, 013407 (2007).
[15] L. Argenti and E. Lindroth, Phys. Rev. Lett. **105**, 053002 (2010).
[16] S. Cavalieri and R. Eramo, Phys. Rev. A **58**, R4263 (1998).
[17] S. N. Pisharody and R. R. Jones, Science **303**, 813 (2004).
[18] D. W. Schumacher, B. J. Lyons, and T. F. Gallagher, Phys. Rev. Lett. **78**, 4359 (1997).
[19] B. J. Lyons, D. W. Schumacher, D. I. Duncan, R. R. Jones, and T. F. Gallagher, Phys. Rev. A **57**, 3712 (1998).
[20] E. Buendía, F. J. Gálvez, P. Maldonado, and A. Sarsa, J. Phys. B **39**, 3575 (2006).
[21] C. J. Joachain, *Quantum Collision Theory* (Elsevier Science, New York, 1984).
[22] R. Wehlitz, D. Lukić, and J. B. Bluett, Phys. Rev. A **68**, 052708 (2003).
[23] NIST Atomic Spectra Database [http://www.nist.gov/physlab/data/asd.cfm].